BULLETIN OF THE POLISH ACADEMY OF SCIENCES
TECHNICAL SCIENCES, Vol. 69(1), 2021, Article number: e136217
DOI: 10.24425/bpasts.2020.136217

VARIA

Longitudinal automatic carrier-landing control law rejecting disturbances and coupling based on adaptive dynamic inversion

Lipeng WANG[1], Zhi ZHANG[1], Qidan ZHU[1], and Zixia WEN[2]

[1] College of Intelligent Systems Science and Engineering, Harbin Engineering University, Harbin, 150001, China
[2] AVIC Xi'an Flight Automatic Control Research Institute, Xi'an, 710065, China

Abstract. The longitudinal automatic carrier landing system (ACLS) control law is designed based on nonlinear dynamic inversion (NDI), which can reject air wake, decouple lateral states, and track the dynamic desired touchdown point (DTP). First of all, the nonlinear landing model of F/A−18 aircraft in the final approach is established, in which the parameters of the aerodynamic, control surfaces, and limited states are acquired. Second, the strategy of tracking the desired longitudinal trajectory through pitch angle control is adopted. The automatic power compensation system (APCS), pitch angle rate, pitch angle, and vertical position control loops are developed based on the adaptive NDI. The stable analysis and the principal description are derived in detail. Deck motion compensation (DMC) algorithm is designed by frequency response method. Third, the control parameters are optimized through the genetic algorithm. A fitness function integrated with velocity, angle of attack (AOA), pitch rate, pitch angle, and vertical position of the aircraft are proposed. Finally, integrated simulations are conducted on a semi-physical simulation platform. The results indicate that the adopted automatic landing control law can achieve both excellent performance and the ability to reject the air wake and lateral coupling.

Key words: carrier-based aircraft; automatic landing; nonlinear dynamic inversion; lateral decoupling; parameters adaptation.

1. Introduction

There are plenty of dangers for the carrier-based aircraft in terminal carrier approach. Nowadays, the landing operations are completed mainly by human pilots. However, a successful recovery mission is accomplished due to some factors, including good visibility, excellent psychological quality, and so on. According to statistical data, more than 70% of fatal aviation accidents can be attributed to human pilots [1]. 11 Class–A hazards in the U.S. Navy were caused by the faulty manipulations of pilots from 2011 to 2012 [2]. Especially in poor landing conditions, artificial manipulations easily lead to serious collision accidents during carrier landing [3]. Therefore, in the 1950s, U.S. Navy planned to design ACLS to enhance the landing safety and improve the landing quality. Not only the difficult landing mission can be completed in a harsher environment, but also the effect of human pilots can be reduced in the recovery operation. At the same time, ACLS can provide more time for filling the ammunition of the aircraft, which can increase the fighting capacity. ACLS will be the main landing form in future, and it is necessary to design a reliable and effective ACLS control law.

Many scholars tried to utilize different methods to establish the ACLS control law. The traditional control law included loops of the position, attitude angle, and attitude angle rate. The control parameters were designed by the PID method. The time and frequency characteristics were easily analyzed by this approach [4]. Backstepping technique was introduced to establish a new automatic carrier landing controller. The performance constraints could guarantee tracking the errors within the prescribed convergence rates [5]. Zhen et al. proposed an ACLS control law by optimal preview control method, in which deck motion was forecasted to acquire the desired glideslope based on particle filtering [6, 7]. H-inf and dynamic inversion were combined to establish an ACLS control law [8]. The air wake and the states measurement deviations were clearly rejected by the robust control approach. Neural network and PID were integrated to develop the glideslope controller for the land-based aircraft [9]. Similarly, neural network was introduced to build a guidance law in the lateral direction in [10]. Bian et al. utilized a modified particle swarm and damped BFGS methods to design the ACLS guidance law [11]. A few researchers used backstepping technology integrating intelligent control ways to increase the stability [12].

The ACLS control law is established by an adaptive super-twisting control method, parameter adjustment and sliding mode differentiators [13]. Likewise, a model reference adaptive control was used to design the ACLS guidance law [14], which can deal with the coupling of all loops and uncertainty of parameters. Some scholars proposed model predictive control [15–17], quantitative feedback theory [18], DOB-based neural control [19, 20], brainstorm optimization [21], and pigeon-inspired optimization [22].

NDI is more convenient in a general way. An L1 adaptive controller with NDI was developed for unmanned aerial vehicle landing [23]. The inner and outer loops were respectively designed by attitude angle rates and position deviations. A Kalman filter integrated with an incremental NDI module

*e-mail: wanglipeng@hrbeu.edu.cn

Manuscript submitted 2020-10-10, revised 2020-12-02, initially accepted for publication 2020-12-05, published in February 2021

was adopted to form landing guidance law, which can suppress the wind disturbance effectively [24]. Bouadi et al. proposed a new ACLS control strategy based on NDI to deal with different kinds of air wake perturbance [25]. Menon et al. utilized the feedback linearization method to design the control law to guide the impaired aircraft [26]. Chen et al. introduced a state observer into the NDI controller and the performance was described in time and frequency domains [27]. Hameduddin et al. raised a tracking desired glideslope path method based on NDI, the stability of the control loops was analyzed in detail [28]. Lungu et al. used NDI in combination with H-inf, state observer, fuzzy controller, or neural network to establish the lateral and longitudinal ACLS control law [29–31].

The traditional NDI method for establishing the ACLS control law is hardly able to deal with the coupling of longitudinal and lateral landing states and the air wake disturbances. Therefore, an innovative robust NDI with adaptive parameter to build ACLS control law is proposed by this paper. On one hand, the lateral landing states are introduced into the longitudinal control loop, which can eliminate air wake and decouple the lateral disturbance. On the other hand, the control parameters are adjusted based on a parameter template to increase the controller's accuracy under the condition of air wake uncertainty.

The rest of the paper is structured as follows. The longitudinal nonlinear landing model of F/A−18 aircraft is constructed in Section 2. The APCS algorithm is built by NDI in Section 3. The ACLS control law in longitudinal direction is designed in Section 4. The DMC method is set up in Section 5. The stability analysis and strategy of control parameters adaptation is described in Section 6. Simulations are presented on a semi-physical platform in Section 7. Section 8 concludes the whole paper.

2. Nonlinear model of aircraft and landing environment

The physical parameters and aerodynamic data of F/A−18 in this paper are sourced from the national aeronautics and space administration [32, 33]. The parameters of F/A−18 are shown in the Table 1.

Table 1
Aircraft parameters of F/A−18 Hornet

Parameters names	Numerical values
Wing area (ft^2)	400
Mean aerodynamic chord (ft)	11.52
Wing span (ft)	37.42
Mass (slugs)	1034.5
Moment of inertia around rolling(slugs)	23000
Moment of inertia around pitch(slugs)	151293
Moment of inertia around yaw(slugs)	169945

The parameters of F/A−18 surface are shown in Table 2.

Table 2
Control surface and actuator configuration

Surface	Velocity constraint (deg/s)	Surface constraint (deg)
Elevator	±40	[−24, +30.5]
Aileron	±100	[−25, +45]
Rudder	±61	[−30, +30]

The dynamic model with the 9 states of F/A−18 is

$$\dot{x} = f(x,u), \tag{1}$$

where, the landing states x includes: approach velocity V; AOA α; sideslip angle β; roll angle ϕ; pitch angle θ; yaw angle ψ; roll rate p; pitch rate q; yaw rate r. The control variables are aileron deflection δ_{ail}, elevator deflection δ_{stab}, and rudder deflection δ_{rud}.

The derivative equation of the Euler angle change is

$$\begin{bmatrix} \dot{\phi} \\ \dot{\theta} \\ \dot{\psi} \end{bmatrix} = \begin{bmatrix} 1 & \sin\phi\tan\theta & \cos\phi\tan\theta \\ 0 & \cos\phi & -\sin\phi \\ 0 & \sin\phi\sec\theta & \cos\phi\sec\theta \end{bmatrix} \begin{bmatrix} p \\ q \\ r \end{bmatrix}. \tag{2}$$

The force equation of F/A−18 about aerodynamic, gravity and thrust can be shown below

$$\begin{cases} \dot{V} = -\frac{1}{m}(D\cos\beta - Y\sin\beta) + \\ \quad g(\cos\phi\cos\theta\sin\alpha\cos\beta + \sin\phi\cos\theta\sin\beta - \\ \quad \sin\theta\cos\alpha\cos\beta) + \dfrac{T}{m}\cos\alpha\cos\beta \\ \dot{\alpha} = -\dfrac{1}{mV\cos\beta}L + q - \tan\beta(p\cos\alpha + r\sin\alpha) + \\ \quad \dfrac{g}{V\cos\beta}(\cos\phi\cos\theta\cos\alpha + \sin\alpha\sin\theta) - \dfrac{T\sin\alpha}{mV\cos\beta}, \\ \dot{\beta} = \dfrac{1}{mV}(Y\cos\beta + D\sin\beta) + p\sin\alpha - r\cos\alpha + \\ \quad \dfrac{g}{V}\cos\beta\sin\phi\cos\theta + \dfrac{\sin\beta}{V}(g\cos\alpha\sin\theta - \\ \quad \sin\alpha\cos\phi\cos\theta + \dfrac{T}{m}\cos\alpha) \end{cases} \tag{3}$$

where T is thrust; D, L and Y are aerodynamic drag force lift force, and side force. m is the mass of aircraft. g is acceleration of gravity. The moment equation is

$$\begin{bmatrix} \dot{p} \\ \dot{q} \\ \dot{r} \end{bmatrix} = \begin{bmatrix} I_{zz}/k & 0 & I_{xz}/k \\ 0 & 1/I_{yy} & 0 \\ I_{xz}/k & 0 & I_{xx}/k \end{bmatrix} \left(\begin{bmatrix} l \\ M \\ n \end{bmatrix} - \begin{bmatrix} 0 & -r & q \\ r & 0 & -p \\ -q & p & 0 \end{bmatrix} \begin{bmatrix} I_{xx} & 0 & -I_{xz} \\ 0 & I_{yy} & 0 \\ -I_{xz} & 0 & I_{zz} \end{bmatrix} \begin{bmatrix} p \\ q \\ r \end{bmatrix} \right), \tag{4}$$

where I_{xx}, I_{yy} and I_{zz} are the moment of inertia around the rolling, pitch, and yaw axes, respectively. I_{xz} is a multiplication

cross of the product of inertia around pitch axis. $k = I_{xx}I_{zz} - I_{xz}^2$. l, M and N are the roll, pitch, and yaw moments.

The aerodynamic force and moment of F/A−18 is concerned with AOA, sideslip angle, angle rate, aileron deflection, elevator deflection, and rudder deflection. The kinetic model of F/A−18 can be described by the following function

$$\begin{cases} D = \overline{q}SC_D(\alpha,\beta,\delta_{stab}), \\ L = \overline{q}SC_L(\alpha,\beta,\delta_{stab}), \\ Y = \overline{q}SC_Y(\alpha,\beta,\delta_{ail},\delta_{rud}), \\ l = \overline{q}SbC_L(\alpha,\beta,\delta_{ail},\delta_{rud},p,r,V), \\ M = \overline{q}SC_L(\alpha,\delta_{stab},q,V), \\ n = \overline{q}SbC_n(\alpha,\beta,\delta_{ail},\delta_{rud},p,r,V), \end{cases} \tag{5}$$

where $\overline{q} = \rho V^2/2$ represents the dynamic pressure; ρ is atmospheric density at sea level; C_D, C_L, C_Y, C_l, C_M, C_N represent the corresponding dynamic coefficients. The landing states are controlled by the aileron and elevator in the lateral and longitudinal directions, but the rudder in the lateral loop only control the lateral position.

In this paper, it is assumed that all landing states can be measured or observed in this paper.

3. Approach power compensation system control law based on NDI

APCS is an independent control loop to maintain constant speed for the aircraft. Most scholars usually design the APCS control law only based on the longitudinal states. However, the coupling from the lateral states is one of the important problems for the stability of the AOA. The roll angle of the aircraft may generate instability in the AOA. An NDI method is adopted by this paper to establish the APCS control law, which integrates the states of the longitudinal and lateral directions. The affine nonlinear equation of the F/A−18 can be represented

$$\begin{cases} \dot{x} = f(x) + g(x)u, \\ y = h(x), \end{cases} \tag{6}$$

where $h(x) = \alpha$. AOA is controlled by the thrust and thrust T is not included in $h(x)$ so the derivative of $h(x)$ with respect to time can be shown

$$\dot{\alpha} = \frac{\partial h(x)}{\partial x}\dot{x} = \frac{\partial h(x)}{\partial x}f(x) + \frac{\partial h(x)}{\partial x}g(x)T. \tag{7}$$

According to the force equation of F/A–18, the following equation is satisfied

$$T = \frac{mV\cos\beta}{\sin\alpha}\left(-\frac{1}{mV\cos\beta}L + q - \tan\beta(p\cos\alpha + r\sin\alpha) + \frac{g}{V\cos\beta}(\cos\phi\cos\theta\cos\alpha + \sin\alpha\sin\theta) - \dot{\alpha}\right). \tag{8}$$

This paper defines the thrust control law as follows

$$T = \frac{mV\cos\beta}{\sin\alpha}\left(-\frac{1}{mV\cos\beta}L + q - \tan\beta(p\cos\alpha + r\sin\alpha) + \frac{g}{V\cos\beta}(\cos\phi\cos\theta\cos\alpha + \sin\alpha\sin\theta) - \dot{\alpha}_{cmd} + v_\alpha\right), \tag{9}$$

where α_{cmd} is the reference control input; v_α is the auxiliary control input, which has to be determined. According to Eq. (9), there is $e_\alpha = \alpha - \alpha_{cmd}$, and the proposed control law is as follows

$$v_\alpha = K_{p1}e_\alpha + K_{I1}\int_0^t e_\alpha \, \mathrm{d}\tau. \tag{10}$$

4. Longitudinal ACLS control law for NDI

Pitch angle mode is utilized by this paper to design the ACLS control law based on NDI. The control law includes three loops: the attitude angle rate loop, the pitch angle loop, and the trajectory loop. The scheme block of the designed system is shown below (Fig. 1).

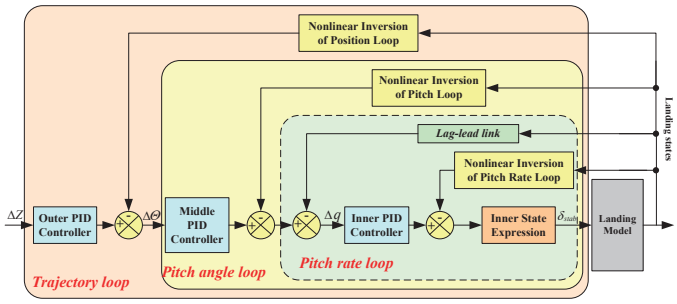

Fig. 1. Scheme block of the designed system

The pitch rate loop, pitch angle loop, and trajectory loop are designed one by one. The nonlinear inversion of the pitch rate is expressed, and the inner PID controller provides the elevator deflection based on pitch rate error. The pitch angle loop calculates the desired pitch rate depending on the middle PID controller and nonlinear inversion of the pitch rate loop. The trajectory loop calculates the desired pitch angle on the basis of outer PID controller and nonlinear inversion of position loop.

4.1. Design of the inner loop in ACLS. The attitude angle rate loop maintains the control augment stability, which provides appropriate angle rate damping. In order to guarantee a rapid and accurate response of the inner loop and minimize the effect of the lateral states, an NDI method is used to establish the inner loop in ACLS.

Eq. (4) can be transformed by the following form

$$\dot{q} = \frac{1}{I_{yy}}\left[M - (I_{xx} - I_{zz})pr - I_{xz}(p^2 - r^2)\right], \tag{11}$$

$$M = \overline{q}S\overline{c}C_M(\alpha, \delta_{stab}, q, V). \tag{12}$$

$C_M(\alpha, \delta_{stab}, q, V)$ includes C_{Mbsc}, C_{Mctrl}, and C_{Mq}, which is shown below

$$\begin{cases} C_{Mbsc} = C_{M_\alpha_2}\alpha^2 + C_{M_\alpha 1}\alpha + C_{M_\alpha 0}, \\ C_{Mctrl} = (C_{M_\delta_{stab2}}\alpha^2 + C_{M_\delta_{stab1}}\alpha + C_{M_\delta_{stab0}})\delta_{stab}, \\ C_{Mq} = (C_{Mq_3}\alpha^3 + C_{Mq_2}\alpha^2 + C_{Mq_1}\alpha + C_{Mq0})q\overline{c}/(2V), \end{cases} \tag{13}$$

where $C_{M_\alpha_2}$, $C_{M_\alpha 1}$, $C_{M_\alpha 0}$, $C_{M_\delta_{stab2}}$, $C_{M_\delta_{stab1}}$, $C_{M_\delta_{stab0}}$, C_{Mq_3}, C_{Mq_2}, C_{Mq_1}, and C_{Mq0} are aerodynamic coefficients.

Eqs. (12) and (13) are substituted into (11), and there is a following equation

$$\begin{aligned} \delta_{stab} = & \frac{1}{\overline{q}S\overline{c}(C_{M_\delta_{stab2}}\alpha^2 + C_{M_\delta_{stab1}}\alpha + C_{M_\delta_{stab0}})} \\ & \big[I_{yy}\dot{q}_{cmd} - I_{yy}v_q - \overline{q}S\overline{c}(C_{M_\alpha_2}\alpha^2 + C_{M_\alpha 1}\alpha + C_{M_\alpha 0}) + \\ & \overline{q}S\overline{c}(C_{M_q_3}\alpha^3 + C_{M_q_2}\alpha^2 + C_{M_q_1}\alpha + C_{M_q0})q\overline{c}/(2V) - \\ & (I_{xx} - I_{zz})pr - I_{xz}(p^2 - r^2)\big], \end{aligned} \tag{14}$$

where q_{cmd} is the reference control input; v_q is the auxiliary control input, which has to be determined.

The expression of traditional control augment stability can be seen in [34] in detail. The frequency response curves are shown below (Fig. 2). The closed loop system introduces the APCS in this paper, and lag-lead link is added into the pitch angle feedback loop so that there is a higher gain in range of 1–20 rad/s in the pitch rate loop of NDI, which provides the necessary lead response time and large frequency band response width for the pitch loop.

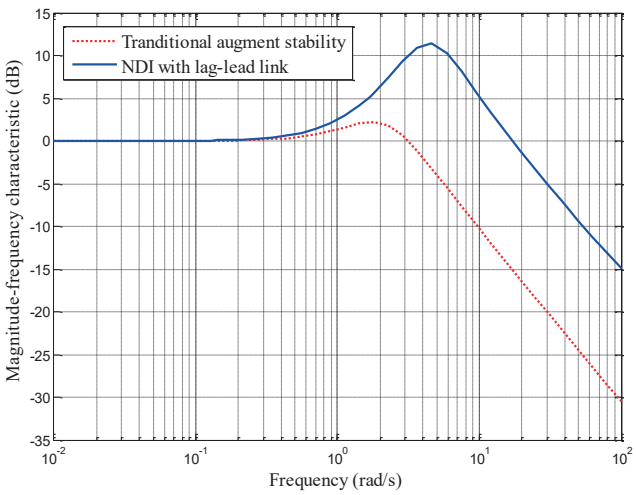

Fig. 2. Bode of pitch rate

According to Eq. (14), there is $e_q = q - q_{cmd}$, and the control law is adopted by this paper as follows

$$v_q = K_{p2}e_q + K_{I2}\int_0^t e_q \,\mathrm{d}\tau. \tag{15}$$

4.2. Design of the middle loop in ACLS. The traditional middle loop is the vertical velocity $\dot{H}$ loop, which is weak due to the coupling of lateral states. This paper adopts the NDI to develop the pitch angle loop.

Based on Eq. (2), this paper defines control law as follows

$$q = \frac{1}{\cos\phi}\left(-v_\theta + r\sin\phi + \dot{\theta}_{cmd}\right), \tag{16}$$

where $\dot{\theta}_{cmd}$ is the reference control input; v_θ is the auxiliary control input, which has to be determined.

It is worth mentioning that the roll angle ϕ on lateral plane is introduced into Eq. (16). The controller can integrate the roll angle into the calculation of the middle loop, and the control algorithm can follow the desired pitch angle order in the presence of lateral disturbance.

According to Eq. (16), there is $e_\theta = \theta - \theta_{cmd}$, and the control law is adopted by this paper as follows

$$v_\theta = K_{p3}e_\theta + K_{I3}\int_0^t e_\theta \,\mathrm{d}\tau. \tag{17}$$

4.3. Design of the outer loop in ACLS. To reject the lateral position coupling, this paper constructs the position control law, and the proposed outer loop control principle is shown below.

According to the relationship between the longitudinal position and pitch angle, longitudinal position components z_g can be shown by

$$\begin{aligned} \dot{z}_g = & -V\cos\beta\cos\alpha\sin\theta + \\ & (V\sin\beta\sin\phi + V\cos\beta\sin\alpha\cos\phi)\cos\theta, \end{aligned} \tag{18}$$

assuming that $\theta = \theta_{trim} + e_\theta$, in which θ_{trim} is equilibrium value of pitch angle at the velocity of 70 m/s, and e_θ is pitch angle deviation. Substituting it into Eq. (18)

$$\begin{aligned} \dot{z}_g = & -V\cos\beta\cos\alpha\sin(\theta_{trim} + e_\theta) + \\ & (V\sin\beta\sin\phi + V\cos\beta\sin\alpha\cos\phi)\cos(\theta_{trim} + e_\theta). \end{aligned} \tag{19}$$

The equation above is linearized at the trim point θ_{trim}, and there is

$$\begin{aligned} \dot{z}_g = f(e_\theta)|_{e_\theta=0} = & (-V\cos\beta\cos\alpha\cos\theta_{trim} - \\ & (V\sin\beta\sin\phi + V\cos\beta\sin\alpha\cos\phi)\sin\theta_{trim})e_\theta = \\ & (-V\cos\beta\cos\alpha\cos\theta_{trim} - \\ & (V\sin\beta\sin\phi + V\cos\beta\sin\alpha\cos\phi)\sin\theta_{trim})(\theta - \theta_{trim}). \end{aligned} \tag{20}$$

The command of θ can be described as

$$\begin{aligned} \theta_{cmd} = & v_{z_g}/(V\cos\beta\cos\alpha\cos\theta_{trim} + \\ & (V\sin\beta\sin\phi + V\cos\beta\sin\alpha\cos\phi)\sin\theta_{trim}) + \theta_{trim}, \end{aligned} \tag{21}$$

where θ_{cmd} is the reference control input; v_{z_g} is the auxiliary control input, which has to be determined.

Substitute Eq. (21) into (20), and the following equation is satisfied

$$\begin{cases} \dot{e}_{z_g} = -v_{z_g}\,, \\ e_{z_g} = z_g - r_{z_g}\,, \end{cases} \tag{22}$$

where e_{zg} is the vertical deviation. This paper adopts the outer loop control v_{z_g} as follows

$$v_{z_g} = k_H e_{zg}\,. \tag{23}$$

The surfaces of the aircraft are easily saturated with large deviations. When pitch angle rate fluctuates, input of the elevator reaches a saturation condition, which results in an unstable aircraft trajectory. The variable gain strategy is adopted by this paper to avoid the saturation of surfaces and thrust. When the initial position deviation is great, the gain of the outer loop controller k_H is decreased. Conversely, k_H is increased. The changing curve of k_H is below (Fig. 3)

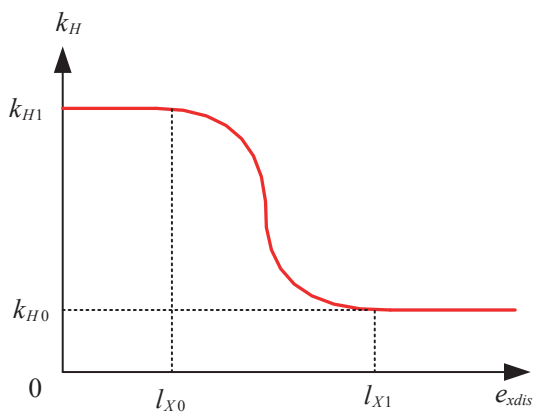

Fig. 3. Time varying weight with respect to approach distance

In the figure above, k_{H0}, k_{H1}, l_{X0}, and l_{X1} are constant values greater than 0. e_{xdis} is the approach distance from the carrier to aircraft.

5. Stability analysis and parameters adaptation

The ACLS control law including Eqs. (10), (15), (17), and (23) is an exponential stable error system. The initial state errors $e_*(0)$ and the first order derivative $\dot{e}_*(0)$ are all 0. Then $e_*(t) = 0$ can be satisfied at any moment through the control strategies. The closed loop system can track the desired states completely. Otherwise, $e_*(t)$ converges exponentially to 0, in which $*$ represents α, q and θ.

According to [34], the control variables of the automatic landing guidance law include different parameters, which play an integrated role for the carrier-based aircraft. Genetic algorithm is adopted to optimize parameters of control law, i.e. K_{p1}, K_{I1}, K_{p2}, K_{I2}, K_{p3} and K_{I3}. The influencing factors of the control effect include the velocity, AOA, pitch rate, pitch angle, and vertical position. A comprehensive fitness function of genetic algorithm is developed by this paper to measure the ACLS control effect. The desired velocity, AOA, pitch rate, pitch angle, and vertical position are represented by V_d, α_d, q_d, θ_d, and P_{zd}. The objective function of ACLS control law $F_{fitness}$ is designed by the following equation

$$F_{fitness} = \int_{t_0}^{t_n} [\omega_1(V(t) - V_d) + \omega_2(\alpha(t) - \alpha_d) + \omega_3(q(t) - q_d) + \omega_4(\theta(t) - \theta_d) + \omega_5(P_z(t) - P_{zd}(t))]\,\mathrm{d}t, \tag{24}$$

where ω_1, ω_2, ω_3, ω_4, and ω_5 are the weight coefficients of each index function. These state deviations are equally important. It is reasonable that the weight coefficients are all set to 1.

The parameters K_{p1}, K_{I1}, K_{p2}, K_{I2}, K_{p3}, and K_{I3} are coded by a real number. This paper utilizes the GA method. The chromosome node includes six factors: $[K_{p1}, K_{I1}, K_{p2}, K_{I2}, K_{p3}, K_{I3}]$. The chromosome node represents a set of control parameters. The range of possible values of chromosome nodes constructs the population M_{pop}. The number of iterations of population evolution is N_{iter}. The crossover, mutation, and selection probabilities are p_{cross}, p_{mut}, and p_{sel}.

This paper adopts the following steps to optimize the parameters above:

Step1. The initial control parameters are determined by artificial choice. If the ACLS control law is stable, the initial parameters are reasonable, and are introduced into the GA method framework.

Step 2. M_{pop} is 100. The chromosome node number of each individual population is 7. The number of iterations of population evolution N_{iter} is 30. p_{cross} and p_{mut} are 0.25 and 0.1.

Step 3. According to a serial of $F_{fitness}$, the least objective function of ACLS control law is chosen as the PID parameters.

The simulation is completed with the initial condition: initial velocity, AOA, pitch rate, pitch angle, vertical deviation as 70.2 m/s, 8.3 deg, 0 deg/s, 4.7 deg, and 15 m, respectively. The difference between the compared simulations is different PID parameters. It is noted that other simulation conditions are same, so that the objective function of ACLS control law is fair. Ten simulation curves are represented as follows based on the steps above. (Figs. 4–9)

According to the simulation result, the control parameters are: $K_{p1} = 0.35$; $K_{I1} = 0.81$; $K_{p2} = 3.5$; $K_{I2} = 10.8$; $K_{p3} = 0.83$; $K_{I3} = 0.72$.

Based on the theory of parameters optimized above, this paper acquires the control parameters under different initial conditions to establish a template. Due to the limited space, taking six landing conditions as an example, the initial conditions and the optimal PID parameters are shown in Tables 3 and 4.

According to Tables 3 and 4, the initial landing states and control parameters establish a high dimension template, which can be simplified by linear interpolation. The real-time landing state deviations can be measured or estimated by observers, so that the initial conditions can be calculated. The control parameters can be found in the template. By this way, the adaptive

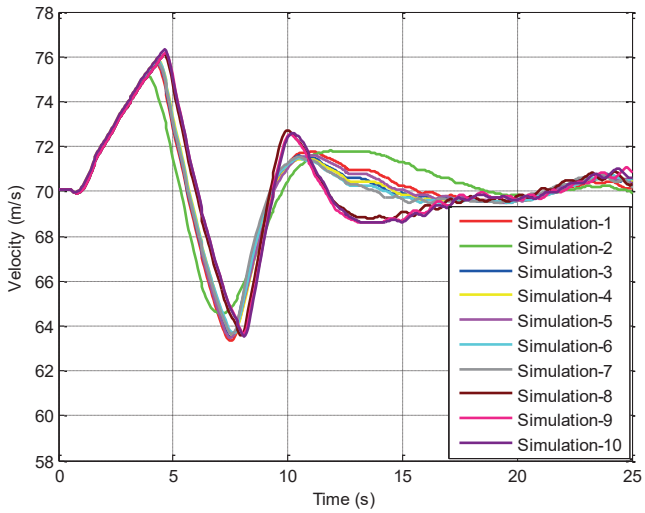

Fig. 4. Velocity curves with different control parameters

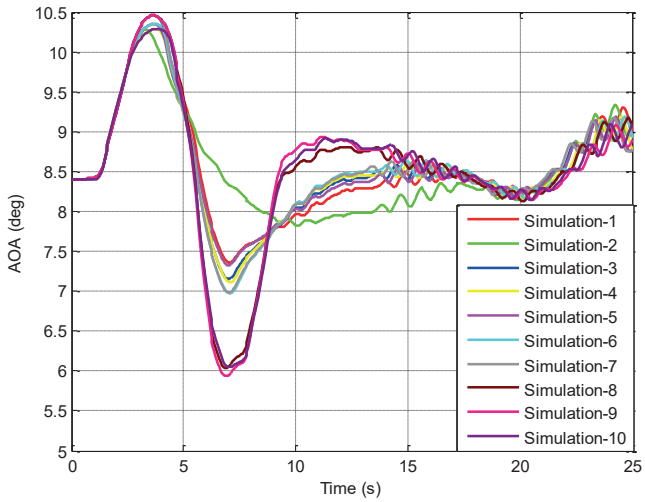

Fig. 5. AOA curves with different control parameters

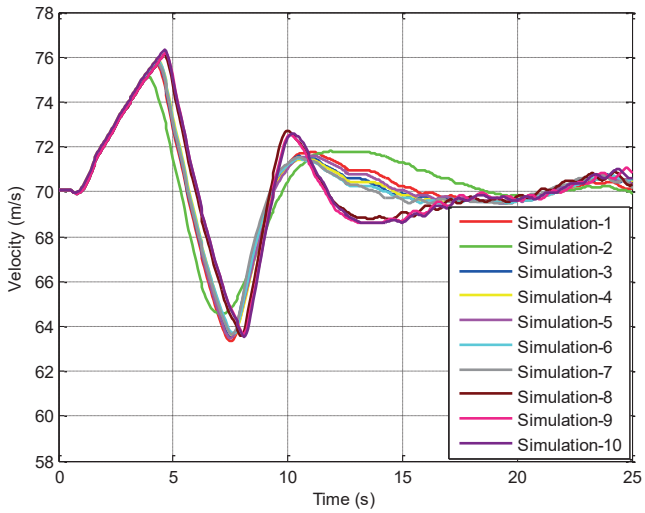

Fig. 6. Pitch rate curves with different control parameters

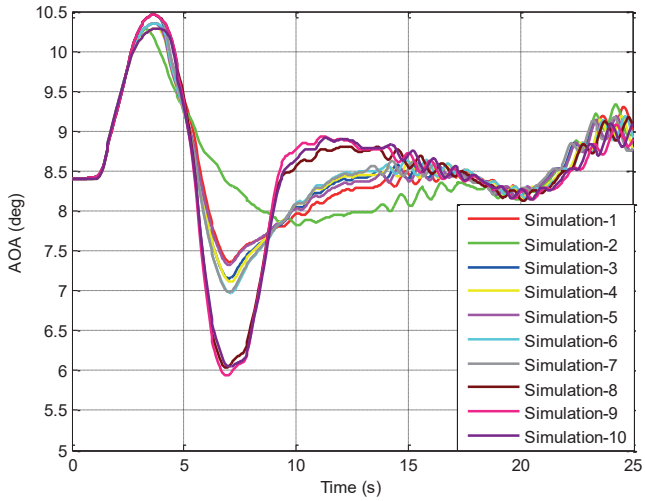

Fig. 7. Pitch angle curves with different control parameters

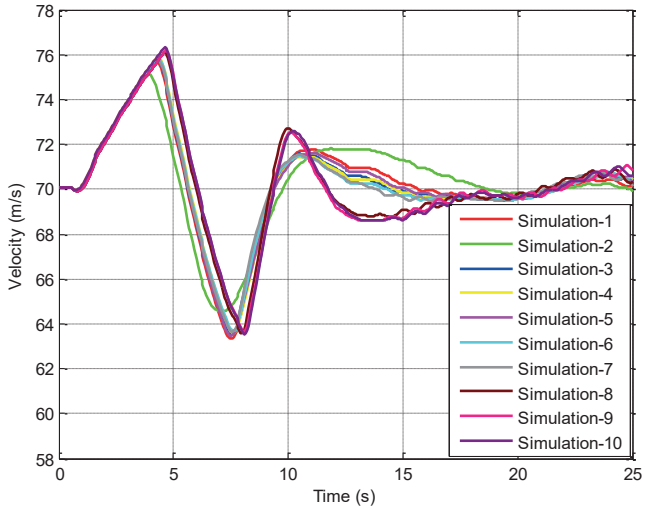

Fig. 8. Vertical deviation curves with different control parameters

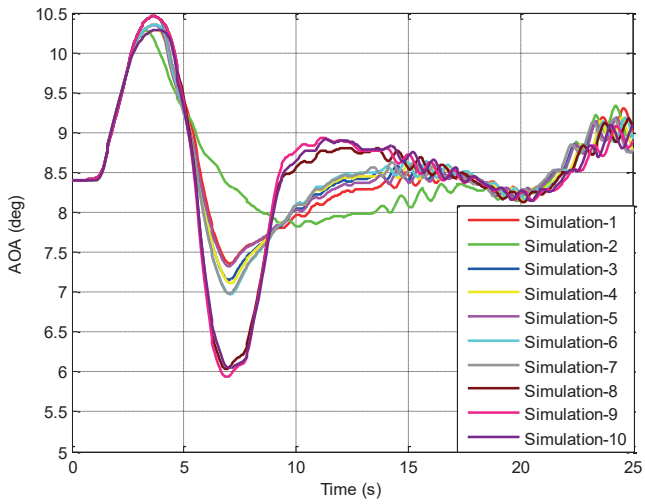

Fig. 9. Evaluation function curves with different control parameters

Table 3
Conditions table in this paper

Conditions	C1	C2	C3	C4	C5	C6
Initial velocity (m/s)	70.2	70.8	70.2	70.2	70.2	70.2
Initial AOA (deg)	8.3	8.3	7.8	8.3	8.3	8.3
Initial pitch rate (deg/s)	0	0	0	0.15	0	0
Initial pitch angle (deg)	4.7	4.7	4.7	4.7	5.1	4.7
Initial vertical deviation (m)	15	15	15	15	15	–15

Table 4
Control parameter template table

Conditions	K_{p1}	K_{I1}	K_{p2}	K_{I2}	K_{p3}	K_{I3}
C1	0.35	0.81	3.5	10.8	0.83	0.72
C2	0.41	0.79	3.44	10.01	0.74	0.74
C3	0.39	0.69	3.96	11.04	0.80	0.83
C4	0.32	0.72	3.14	10.34	0.88	0.89
C5	0.44	0.88	2.97	10.17	0.92	0.64
C6	0.51	0.64	4.11	10.24	0.71	0.57

parameters provide the optimal control effect under different conditions.

In general, the disturbance can be rejected depending on the following ways by the proposed method: (1) The template with adaptive control parameters in Section 5. (2) The nonlinear dynamic inversions in outer, middle, and inner loops considering lateral states in Section 3 and 4.

6. Simulation and analysis

The proposed algorithm is tested on a semi-physical simulation system, which is shown in Fig. 10. In order to verify the effectiveness of the proposed method, this paper utilizes the method from [15] and the NID without considering the lateral coupling for comparison. The nonlinear landing model of F/A-18A, the adaptive NDI control law, and the DMC algorithm are operated by the Visual Studio 2010. The three-dimensional landing scene is realized by Vega Prime 6.0. Data analysis and landing evaluation modules of the final approach phase are programmed by the QT 5.4.2. The simulated information is connected through the network communication.

The integrated simulation is conducted by this section, including the loop of pitch rate, pitch angle, and position in the presence of deck motion and air wake disturbance. The method from this paper is labeled as "The proposed method", and the compared method from [15] is labeled as "The modified MPC method". The NDI without considering lateral coupling is labeled as "with lateral couple". The initial uniform simulation states and the desired states are shown below (Table 5)

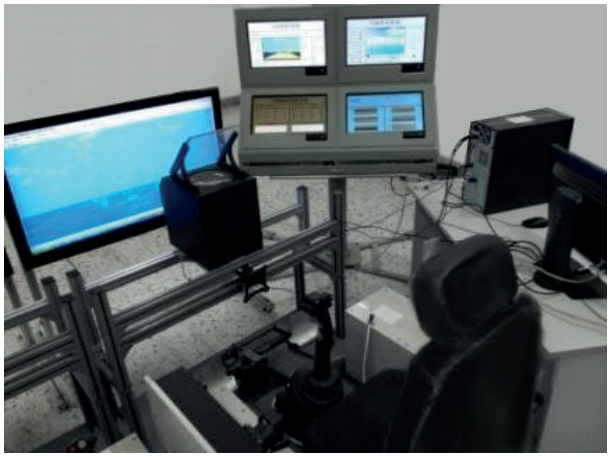

Fig. 10. Semi-physical landing simulation system

Table 5
Control parameter template table

State variables	Initial values	Desired values
Vertical deviation (m)	–8	0
Velocity (m/s)	69.7	70.0
AOA (deg)	9.5	9.4
Pitch angle (deg)	6.0	4.9

The simulation time is 25 s. The sea state is 3. The wind velocity is 4.5 m/s. It is noted that the turbulence is included in the wind condition. The airwake disturbance accords with the military standard. The simulated curves are shown in Figs. 11– 16.

In Fig. 11, the vertical deviation is eliminated by the proposed method more quickly than the compared one. This is due to the adaptive control parameters. In the other aspect, the overshoot of the robust NDI method is lower than the MPC method. On the one hand, the maximal overshoot of the com-

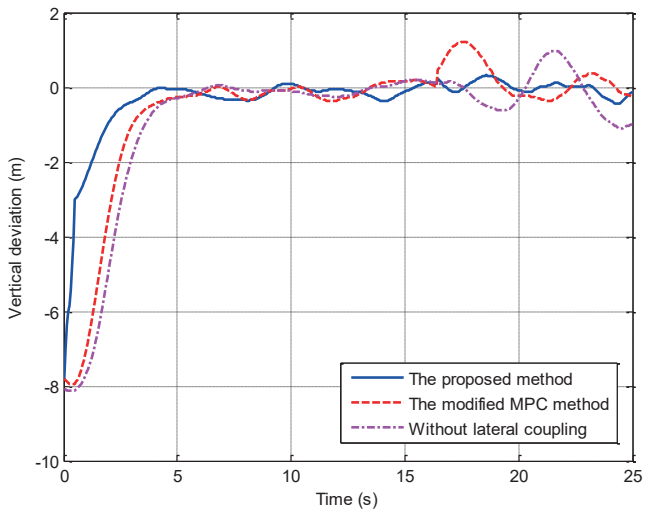

Fig. 11. Vertical deviation curves

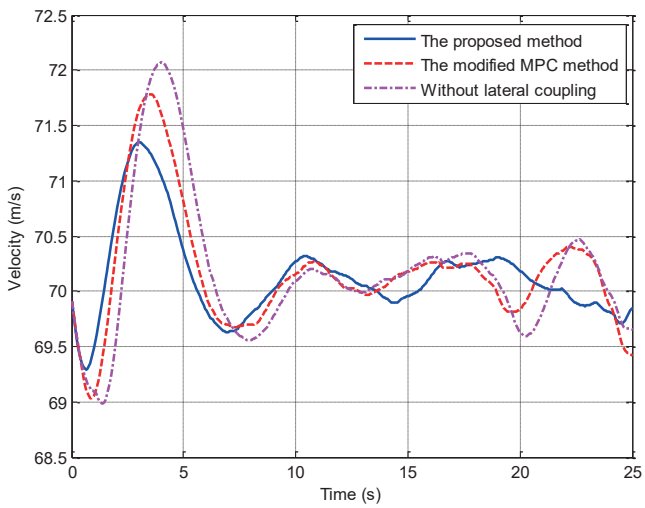

Fig. 12. Velocity curves

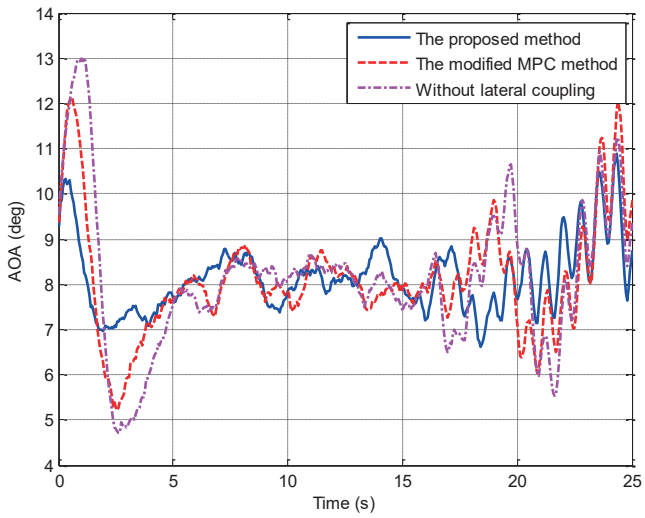

Fig. 13. AOA curves

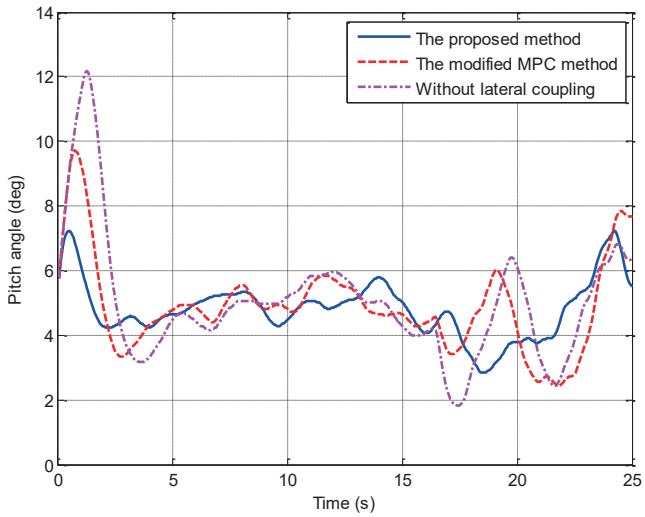

Fig. 14. Pitch angle curves

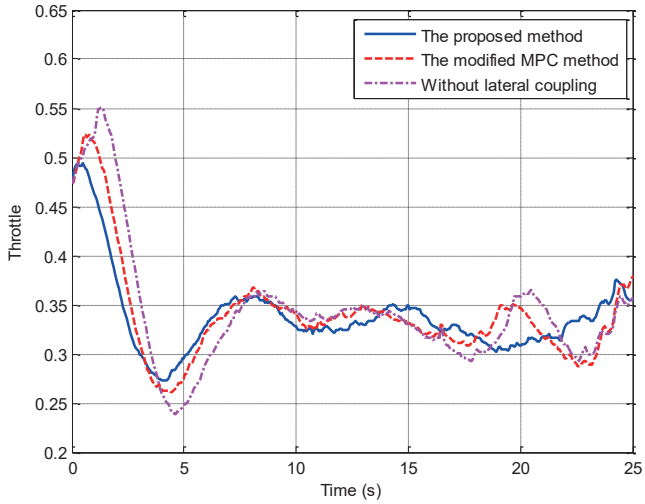

Fig. 15. Throttle curves

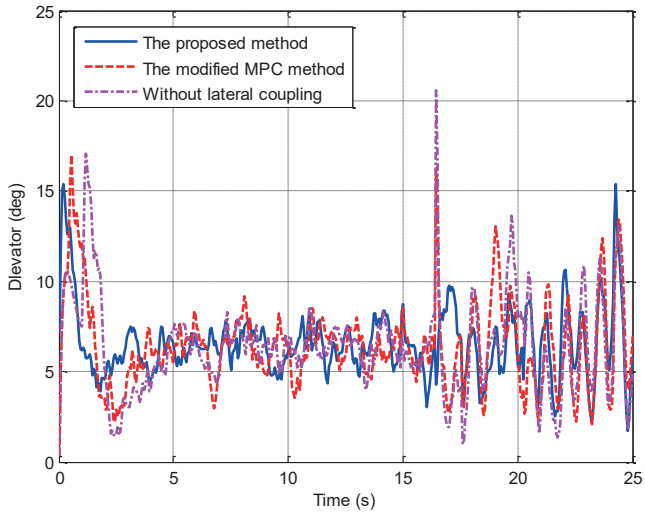

Fig. 16. Elevator control curves

pared method is greater than the proposed method. This is nearby the carrier stern, which is very dangerous for the aircraft. On the other hand, the average overshoot of the compared method is greater than our paper. In other words, the overshoot based on the compared method is clearly seen to be affected by the air wake and deck motion. Therefore, this is dangerously near the carrier stern. It is noted that there is some fluctuation in the vertical deviation of the proposed method. This is caused by the deck motion. The aircraft needs to track the deck motion and adjust the velocity. From Fig. 12. on the one hand, the velocity overshoot is rejected faster by the proposed algorithm. On the other, the velocity fluctuates seriously by the compared method. This is because the air wake disturbs the carrier-based aircraft fiercely at the end of the simulation, i.e. near the stern in the space. Similarly, the AOA curves verify that the control effect of the proposed method is better than the modified MPC method, which can be seen in Fig. 13. It is noted that velocity and AOA do not reach the desired 70 m/s and 8.4 deg, and this is due to the air wake disturbance. The pitch angle curves are rep-

resented by Fig. 14. Though the curves from both methods fluctuate severely due to tracking of deck motion and the rejection of air wake, the overshoot elimination and rapidity of the proposed method is superior to the compared method. The throttle and stabilizer control curves are shown in Figs. 15 and 16. Not only the control amplitude but also control frequency is lower in the NDI method than in the compared method. The energy consumption through the proposed method by this paper is lower than in the modified MPC method. When the aircraft is near the stern, the stabilizer has to generate an additional control value. Therefore, it is reasonable that the stabilizer is controlled frequently. What is more, according to the overshoot and adjustment time curves of the vertical deviation, velocity, AOA, pitch angle, and control outputs, the proposed method is better than the NDI without considering lateral coupling.

To sum up, the control effect by the proposed method outruns the compared method, including robustness, rapidity, energy consumption, and disturbance rejection.

7. Conclusions

This paper establishes a longitudinal loop of trajectory tracking system based on the adaptive NDI method, which can decrease the effectiveness of a lateral loop and reject the air wake. In the end, we reached three conclusions in this study.

First of all, the APCS control law proposed by this paper introduces the lateral state coupling. Therefore, the algorithm can maintain the constant AOA and velocity, and eliminate roll rate and angle coupling. The longitudinal control loop removes the lateral coupling, which increases the robustness of ACLS control law.

Second, the inner, middle, and outer loops were designed, respectively. The stability can be guaranteed in each control loop so that the whole robustness of ACLS control law is ensured. The control curves show that the aircraft can track the dynamics of the desired glideslope with the small deviation.

Third, the control parameter optimization was achieved based on the genetic algorithm. An adaptive control theory is proposed by the control parameter template. The optimal PID parameters were determined by multiple simulations.

Acknowledgements. This work was supported by the National Natural Science Foundation of China (No. 61803116) and supported by the Fundamental Research Funds for the Central Universities of China (No. 3072019CFJ0405, 3072020CF0410).

References

[1] M. Ryota and S. Shinji, "Modeling of pilot landing approach control using stochastic switched linear regression model", *J. Aircr.* 47(5), 1554–1558 (2010).

[2] J. Tian, Y. Dai, H. Rong, and T.D. Zhao, "Hybrid safety analysis method based on SVM and RST: An application to carrier landing of aircraft", *Saf. Sci.* 80, 56–65 (2015).

[3] L.P. Wang, Q.D. Zhu, Z. Zhang, and R. Dong. "Modeling pilot behaviors based on discrete–time series during carrier-based aircraft landing", *J. Aircr.* 53(6), 1922–1931 (2016).

[4] J.M. Urnes and R.K. Hess, "Development of the F/A−18A automatic carrier landing system", *J. Guid.* 8(3), 289-295 (1985).

[5] Z.Y. Guan, Y.P. Ma, and Z.W. Zheng, "Prescribed performance control for automatic carrier landing with disturbance", *Nonlinear Dyn*. 94(2),ţ 1335–1349 (2018).

[6] Z.Y. Zhen, S.Y. Jiang, and K. Ma, "Automatic carrier landing control for unmanned aerial vehicles based on preview control and particle filtering", *Aerosp. Sci. Technol.* 81, 99–107 (2018).

[7] Z.Y. Zhen, S.Y. Jiang, and J. Jiang, "Preview control and particle filtering for automatic carrier landing", *IEEE Trans. Aerosp. Electron. Syst.* 54(6), 2662–2674 (2018).

[8] R. Lungu and M. Lungu, "Design of automatic landing systems using the H-inf control and the dynamic inversion", *J. Dyn. Syst. Meas. Control-Trans. ASME.* 138(2), 1–5 (2016).

[9] R. Lungu and M. Lungu, "Automatic Landing system using neural networks and radio-technical subsystems", *Chin. J. Aeronaut.* 30(1), 399–411 (2017).

[10] M. Lungu and R. Lungu, "Automatic control of aircraft lateral-directional motion during landing using neural networks and radio-technical subsystems", *Neurocomputing.* 171, 471–481 (2016).

[11] Q. Bian, B. Nener, T. Li, and X.M. Wang, "Multimodal control parameter optimization for aircraft longitudinal automatic landing via the hybrid particle swarm-BFGS algorithm", *Proc. Inst. Mech. Eng. Part G-J. Aerosp. Eng*. 233(12), 4482–4491 (2019).

[12] F.Y. Zheng, Z.Y. Zhen, and H.J. Gong, "Observer-based backstepping longitudinal control for carrier-based UAV with actuator faults", *J. Syst. Eng. Electron.* 28(2), 322–337 (2017).

[13] Z.Y. Zhen, C.J. Yu, and S.Y. Jiang, "Adaptive super-twisting control for automatic carrier landing of aircraft", *IEEE Trans. Aerosp. Electron. Syst*. 56(2), 987–994 (2020).

[14] Z.Y. Zhen, G. Tao, and C.J. Yu, "A multivariable adaptive control scheme for automatic carrier landing of UAV", *Aerosp. Sci. Technol.* 92, 714–721 (2019).

[15] L.P. Wang, Z. Zhang, Q.D. Zhu, and R. Dong, "Longitudinal automatic carrier landing system guidance law using model predictive control with an additional landing risk term", *Proc. Inst. Mech. Eng. Part G-J. Aerosp. Eng*. 233(3), 1–17 (2019).

[16] L.P. Wang, Z. Zhang, and Q.D. Zhu, "Automatic Flight Control Design Considering Objective and Subjective Risks during Carrier Landing", *Proc. Inst. Mech. Eng. Part I-J Syst Control Eng.* 234(4), 446–461 (2020).

[17] L.P. Wang, Z. Zhang, Q.D. Zhu, X.W. Jiang, "Lateral autonomous carrier-landing control with high-dimension landing risks consideration", *Aircr. Eng. Aerosp. Technol.* 92(6), 837–850 (2020).

[18] T. Woodbury and J. Valasek, "Synthesis and flight test of an automatic landing controller using quantitative feedback theory", *J. Guid. Control Dyn.* 39(9), 1994–2010 (2016).

[19] B. Xu, D.W. Wang, Y.M. Zhang, and Z.K. Shi, "DOB-based neural control of flexible hypersonic flight vehicle considering wind effects", *IEEE Trans. Ind. Electron.* 64(11), 8676–8685 (2017).

[20] D. Gawel, M. Nowak, H. Hausa, and R. Roszak, "New biomimetic approach to the aircraft wing structural design based on aeroelastic analysis", *Bull. Pol. Ac.: Tech.* 65(5), 741–750 (2017).

[21] J.N. Li and H.B. Duan, "Simplified brain storm optimization approach to control parameter optimization in F/A−18 automatic carrier landing system", *Aerosp. Sci. Technol.* 42, 187–195 (2015).

[22] R. Dou and H.B. Duan, "Levy flight based pigeon-inspired optimization for control parameters optimization in automatic carrier landing system", *Aerosp. Sci. Technol.* 61, 11–20 (2017).

[23] K. Lu and C.S. Liu, "A L-1 adaptive control scheme for UAV carrier landing using nonlinear dynamic inversion", *Int. J. Aerosp. Eng.* 1–9 (2019).

[24] M. Brodecki and K. Subbarao. Autonomous formation flight control system using in-flight sweet-spot estimation. *J. Guid. Control Dyn.* 38(6), 1083–1096 (2015).

[25] H. Bouadi, F.M. Camino, and D. Choukroun, "Space–Indexed Control for Aircraft Vertical Guidance with Time Constraint", *J. Guid. Control Dyn.* 37(4), 1103–1113 (2014).

[26] P.K. Menon, S.S. Vaddi, and P. Sengupta, "Robust landing-guidance law for impaired aircraft", *J. Guid. Control Dyn.* 35(6), 1865−1877 (2012).

[27] W.H. Chen, "Nonlinear Disturbance observer-enhanced dynamic inversion control of missiles", *J. Guid. Control Dyn.* 26(1), 161–166 (2003).

[28] I. Hameduddin and A.H. Bajodah, "Nonlinear generalised dynamic inversion for aircraft manoeuvring control", *Int. J. Control.* 85(4), 437–450 (2012).

[29] R. Lungu and M. Lungu, "Design of automatic landing systems using the H-inf control and the dynamic inversion", *J. Dyn. Syst. Meas. Control-Trans. ASME.* 138(2), 1–5 (2016).

[30] M. Lungu and R. Lungu, "Landing auto-pilots for aircraft motion in longitudinal plane using adaptive control laws based on neural networks and dynamic inversion", *Asian J. Control.* 19(1), 302–315 (2017).

[31] R. Lungu and M. Lungu, "Automatic control of aircraft in lateral-directional plane during landing", *Asian J. Control.* 18(2), 433–446 (2016).

[32] A. Chakraborty, P. Seiler, and G. J. Balasz, "Applications of linear and nonlinear robustness analysis techniques to the F/A-18 flight control laws", AIAA Guidance, Navigation, and Control conference. Chicago, USA, 2009, pp.10–13.

[33] A. Chakraborty, P. Seiler, and G. J. Balas, "Susceptibility of F/A−18 flight controllers to the falling-leaf mode: nonlinear analysis", *J. Guid. Control Dyn.* 34(1), 57–72 (2011).

[34] J.M. Urnes, and R.K. Hess, "Development of the F/A-18A Automatic Carrier Landing System", *J. Guid.* 8(3), 289–295 (1985).